Visualization of Multipolar Longitudinal and Transversal Surface Plasmon Modes in Nanowire Dimers

Ina Alber,[†,*] Wilfried Sigle,[‡] Sven Müller,[†] Reinhard Neumann,[†] Oliver Picht,[†] Markus Rauber,[†,§] Peter A. van Aken,[‡] and Maria Eugenia Toimil-Molares[†,*]

[†]Materials Research Department, GSI Helmholtzzentrum für Schwerionenforschung GmbH, Darmstadt, Germany, [‡]Stuttgart Center for Electron Microscopy, MPI for Intelligent Systems, Stuttgart, Germany, and [§]Department of Materials- and Geo-Sciences, Technische Universität Darmstadt, Darmstadt, Germany

ABSTRACT

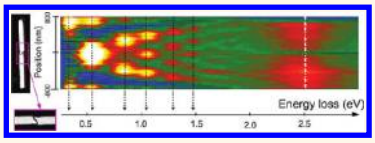

We study the transversal and longitudinal localized surface plasmon resonances in single nanowires and nanowire dimers excited by the fast traveling electron beam in a transmission electron microscope equipped with high-resolution electron energy-loss spectroscopy. Bright and dark longitudinal modes up to the fifth order are resolved on individual metallic nanowires. On nanowire dimers, mode splitting into bonding and antibonding is measured up to the third order for several dimers with various aspect ratio and controlled gap size. We observe that the electric field maxima of the bonding modes are shifted toward the gap, while the electric field maxima of the antibonding modes are shifted toward the dimer ends. Finally, we observe that the transversal mode is not detected in the region of the dimer gap and decays away from the rod more rapidly than the longitudinal modes.

KEYWORDS: transversal surface plasmon resonance · longitudinal surface plasmon resonances · bonding multipol order modes · antibonding multipol order modes · electron energy-loss spectroscopy · nanowire dimer synthesis

Localized surface plasmon resonances (LSPR) in metallic nanostructures are very important for applications such as surface-enhanced Raman spectroscopy (SERS),[1−3] surface-enhanced infrared spectroscopy,[4,5] and waveguiding below the diffraction limit of light .[6,7] A variety of nanostructures have been tested for these applications such as single nanoparticles,[3] nanoshells,[8] and nanowires,[4,5,7,9] as well as ordered arrays,[10−13] and self-assemblies of these structures.[14−16] In the case of nanowires, both longitudinal and transversal LSPR are excitable due to the two different axis lengths of the wires. In particular, the longitudinal resonance frequencies are tunable to a high degree by adjusting wire length and diameter.[17−19] Due to the nanowire geometry, the longitudinal modes generate high absorption and scattering cross sections, and thus large field enhancements.[5,20,21] Additionally, since multipolar modes can be excited efficiently, simultaneous excitation of resonances at several frequencies is possible, using only one nanowire. So far, several authors have evidenced that multipolar resonances in nanowires give rise to SERS efficiencies the same as or higher than the respective dipolar resonances.[12,13] Among all modes, only those having an even number of charge maxima along the wire (bright modes) can couple efficiently to incident far-field radiation. Nevertheless, investigation of modes having an odd number of maxima along the wire (dark modes) is crucial, since coupling to dark modes allows for waveguiding of light, avoiding radiative losses, and can therefore be efficiently employed in nanophotonic devices.[22] Particular interest was most recently focused on the excitation of LSPR in two nanostructures separated by a small gap, so-called nanostructure dimers. In this case, coupling between the LSP modes of the individual structures leads to a splitting of each mode into a bonding and an antibonding mode.[23−27] It is known that gaps of very small size (few nm) are required to generate high-field enhancements in dimer systems.[28] For such a configuration the enhancement factor and resonance frequency depend on numerous parameters such as wire aspect ratio, gap size, and wire material and morphology. Although the near-field multipolar resonance excitation of single gold and silver nanowires has been discussed recently,[29−32] similar measurements of multipolar resonances on elongated nanowire dimers have, to the best of our knowledge, not been reported so far. In addition, measurements employing gaps

* Address correspondence to i.alber@gsi.de; m.e.toimil-molares@gsi.de.

Received for review September 12, 2011 and accepted November 11, 2011.

Published online November 11, 2011
10.1021/nn2035044

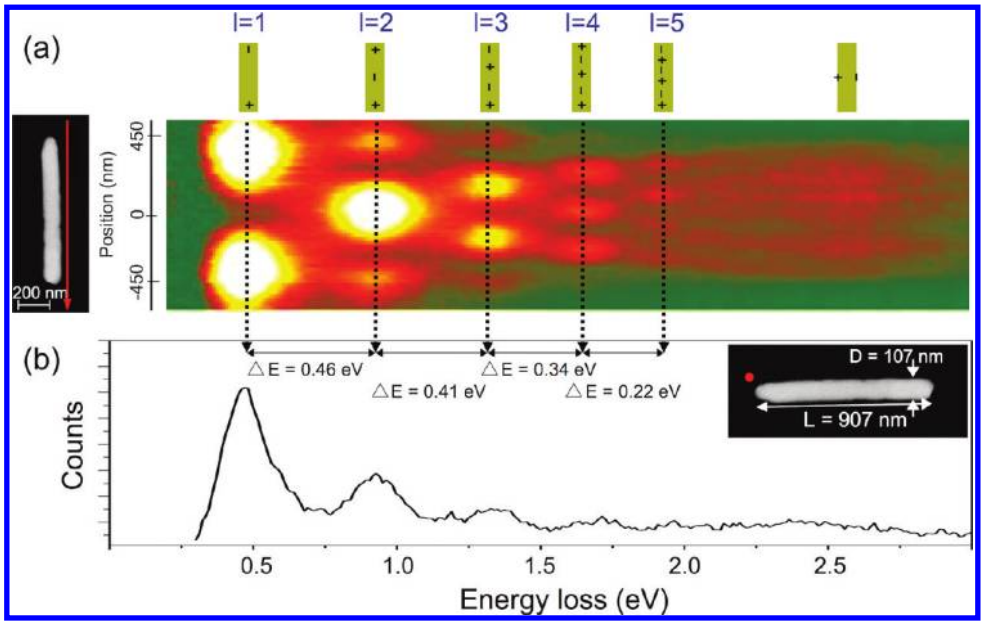

Figure 1. (a) High-resolution plasmonic field intensity map consisting of 50 electron energy-loss spectra measured along the long axis of a nanowire in the direction of the arrow on the left. The energy interval, plotted from left to right, ranges from 0.2 to 3.0 eV. The color indicates the number of counts. The average distance of the scan line to the nanowire is ~15 nm. (b) Electron energy-loss spectrum measured at one end of the single nanowire. The inset shows a TEM image of the single nanowire corresponding to the spectrum. The red dot marks the position of measurement.

smaller than 15 nm are rare due to difficulties in the preparation processes.

Here, we present scanning transmission electron microscopy (STEM) imaging combined with electron energy-loss spectroscopy (EELS) of LSPR coupling in metallic nanowire dimers with gap sizes down to about 7 nm. Applying this method we investigate bright and dark longitudinal as well as transversal modes with a very high spatial resolution of a few nanometers. A high-energy resolution of ~0.12 eV enabled the study of mode splitting into bonding and antibonding modes, amounting to 0.23 eV for a gap of about 8 nm. The influence of gap size, aspect ratio, and multipole order on mode splitting is discussed. Finally, we investigate the spatial charge distribution along the single nanowire as well as the nanowire dimer for bonding and antibonding modes.

RESULTS AND DISCUSSION

Figure 1a shows the high-resolution plasmonic field intensity map obtained by acquisition of 50 electron energy-loss spectra at equispaced positions along the long axis of a gold silver alloy nanowire with length L = 907 ± 5 nm and diameter D = 107 ± 5 nm. The single nanowire as well as the nanowire dimers discussed later are referred to as gold wires in the following, since we assume that due to the preparation process the amount of residual Ag close to the surface of the wire is very small and thus the silver content influences the resonance energies only slightly (see Methods). The spectra were acquired from top to bottom as indicated by the red arrow in the TEM image of the wire. The average distance of the scan line to the nanowire is ~15 nm. From left to right, the energy loss increases from 0.2 to 3.0 eV. The color scale indicates the number of counts, representing the probability of electron-surface plasmon inelastic scattering, and results in a spatial representation of the plasmon modes resolved at different energy losses. The map reveals six different plasmon modes. We assign the first five modes in the spectra to the first five longitudinal LSP modes. In analogy to a Fabry-Pérot resonator, the surface plasmon wavelength λ_{SP} is given by

$$\lambda_{SP} = \frac{2}{l - \frac{\delta\Phi}{\Pi}} L \qquad (1)$$

where L is the length of the nanowire, l is the multipole order starting with l = 1 for the dipolar LSPR and l = 2, 3, 4 for higher multipole order resonances, and $\delta\Phi$ represents a phase jump upon reflection at the nanowire ends.[29] On top of Figure 1a the electric field distribution along the wire for the five longitudinal multipole modes is schematically presented. An additional mode is visible in the map, which is excitable when positioning the electron beam on any point on the scan line along the nanowire (red arrow), but decays rapidly beyond the wire ends. Its energy, centered at ~2.6 eV, is in reasonable agreement with previously reported energy values of the transversal surface plasmon resonance in gold nanorods, namely, 2.4 and 2.5 eV.[34,35] In our case, the shift of the transversal mode to slightly higher energies can be attributed to a certain amount of silver remaining in the wire

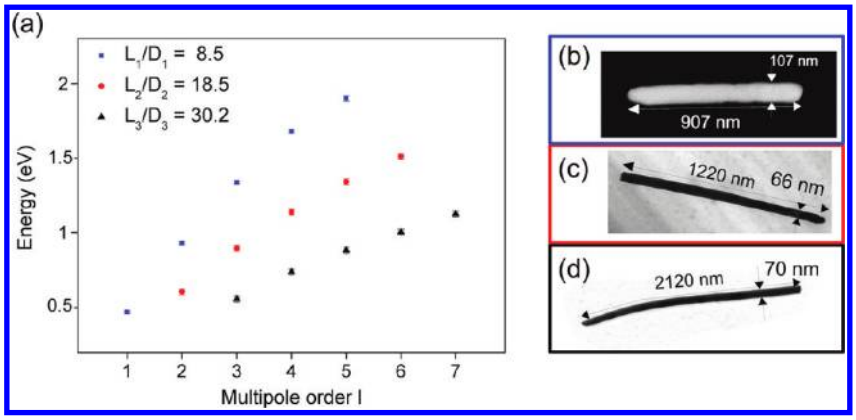

Figure 2. (a) Resonance energies of the multipole longitudinal LSP modes for three wires with different aspect ratios. The TEM images (b), (c), and (d) show the wires. The colors of the frames adopt those of the values in (a).

after the preparation process (see Methods). Figure 1b shows a single spectrum of the mapping in Figure 1a, recorded at one side-end of the nanowire (red dot in inset). The spectrum reveals energy-loss peaks for at least the first four LSP modes from the mapping at 0.47 ± 0.01, 0.93 ± 0.01, 1.34 ± 0.01, and 1.68 ± 0.01 eV, also visualized in the mapping in Figure 1a.

Figure 1a and b evidence that with increasing *l* the intensity of the peaks decreases, as shown in previous publications.[36] The energy-loss probability depends on the interaction between the electrons and the induced electric field. Thus, for the first-order LSP resonance, the high electric field at the side-end of the wires comes along with a high energy-loss probability.[37] With increasing multipole order, the surface plasmon wavelength according to eq 1 decreases, and thus also the separation distance between positive and negative electric field maxima. Hence, the induced electric field represented by the loss probability drops.[18,28] In addition, damping from interband transitions increases with energy and renders higher order longitudinal modes than $l = 5$, not distinguishable in the spectrum.[38] The energy difference ΔE, given in Figure 1b and determined from Figure 1a, specifies the distances between two consecutive longitudinal modes. Noticeably, with increasing energy loss, ΔE decreases from $\Delta E = 0.46 \pm 0.02$ eV for the difference between the $l = 1$ and $l = 2$ modes to $\Delta E = 0.22 \pm 0.03$ eV for the difference between the $l = 4$ and $l = 5$ modes.

The resonance energies of the different multipole modes of three nanowires with different length and diameter are plotted in Figure 2a. The three wires and their respective dimensions are displayed in the TEM images in Figure 2b–d: the nanowire shown in Figure 1 with $L_1 = 907 \pm 5$ nm, $D_1 = 107 \pm 5$ nm, and aspect ratio $L_1/D_1 = 8.5$ (blue squares) (Figure 2b), a thinner wire with $L_2 = 1220 \pm 5$ nm, $D_2 = 66 \pm 10$ nm, and aspect ratio $L_2/D_2 = 18.5$ (red circles) (Figure 2c), and a longer wire with $L_3 = 2120 \pm 10$ nm, $D_3 = 70 \pm 5$ nm, and aspect ratio $L_3/D_3 = 30.2$ (black triangles) (Figure 2d). The two longer wires (Figure 2c and d) were deposited from an electrolyte containing only gold cyanide ions, and their electron energy-loss spectra were measured with a less focused electron beam having a diameter of about 140 nm.

For all three wires, a decrease in the energy difference between two consecutive modes with increasing energy is evident. The energy values in Figure 2a reveal that the longer the nanowire, the larger the spatial separation between field maxima for a specific mode and the smaller the restoring force responsible for the plasmonic oscillation, resulting in a lower energy for each given mode.[28] We observe that the LSPR energies for the wire corresponding to Figure 1 (blue squares) are higher than the ones for the two wires in Figure 2c and d. Besides the shorter length of this wire, also its silver content and increased diameter play a role.[18,21] Our results evidence that the shifts in resonance energy due to wire length, diameter, and composition may be properly investigated by STEM-EELS.

Figure 3a shows a high-resolution plasmonic field intensity map of a dimer of two nanowires separated by a gap of only ~8 nm. These two wires have lengths of about 784 ± 5 and 808 ± 5 nm, respectively. The diameter of both wires is 112 ± 5 nm. The intensity map is composed of two one-dimensional line scans. Each of them consists of 30 equidistantly spaced electron energy-loss spectra measured along the long axis of one of the wires forming the dimer, as indicated by the red arrow, to ensure an almost constant distance of the scan from the wire, which is on average ~10 nm (see TEM image in Figure 3a). From left to right the energy loss varies from 0.25 to 3.0 eV. The colors indicate the number of counts and thus visualize the spatial distribution of the LSP modes along the one-dimensional scan.

Figure 3b displays three spectra recorded at different positions of the dimer: the blue and green spectra were measured by placing the focused electron beam (few nanometers spot size) at the dimer ends, while the red spectrum was taken by placing the focused electron beam at the dimer gap. The corresponding

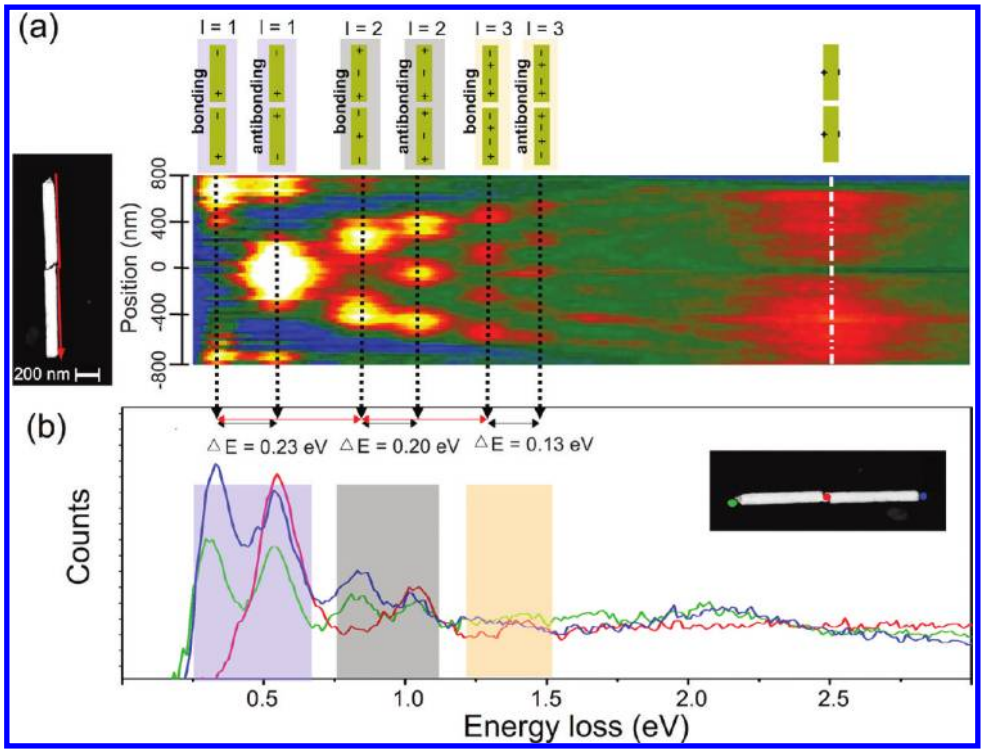

Figure 3. (a) Plasmonic field intensity map consisting of 60 electron energy-loss spectra measured along a nanowire dimer (red arrow). The scan lines have an average distance to the wire of ~10 nm. The wires are separated by a small gap of ~8 nm. The energy interval, plotted from left to right, ranges from 0.25 to 3.0 eV. The color represents the count number. The schematics on top represent the electric field distribution along the dimer. (b) Electron energy-loss spectra measured at the two ends of the dimer (blue and green lines) and a spectrum measured in the dimer gap (red line). The colored dots in the TEM image inset specify the measurement positions for each spectra.

colored dots in the TEM image of the inset specify the measurement positions of the respective spectra. The two spectra measured at the ends of the dimer (green and blue spectra) differ in intensity since they are not measured exactly at the same positions relative to the dimer ends (see TEM image in Figure 3b).

In Figure 3a at least six low-energy modes of longitudinal character are visible. The LSP intensity map of the dimer can be clearly distinguished from that of a single nanowire when looking at the energy difference between two consecutive longitudinal modes. For the single nanowire a continuous decrease in energy difference with increasing multipole order is observed (see Figures 1 and 2). In the case of the dimer, we observe that the modes can be separated into three pairs, each pair having a smaller energy difference than the differences to neighboring pairs. It is well-known that the small gap of about 8 nm enables the coupling between LSPR of the two individual nanowires, leading to a splitting of the modes into a bonding mode and an antibonding mode.[24−27] For each multipole order the bonding and antibonding mode forms one of the observed mode pairs. The schematics on top represent the electric field distribution along the wire for each bonding and antibonding mode (purple for $l = 1$, gray for $l = 2$, and orange for $l = 3$). In Figure 3b each mode pair is highlighted with the same color for further clarification. The bonding mode corresponds to a charge distribution where charge carriers of opposite sign are accumulated at opposite gap ends. In contrast, the antibonding mode is excited when charge carriers of the same sign repel each other at the two gap sides. The attraction between negative and positive charge carriers at the two gap sides leads to a decrease in restoring force and thus to a shift in energy of the bonding mode to lower energies compared to the antibonding mode. We observe splitting into bonding and antibonding not only for the dipolar mode but also up to at least the third-order mode. The peaks corresponding to multipole orders higher than three at the two ends of the dimer are not visible in the spectra due to their low intensity but can be resolved at different color scaling. Figure 3a and b evidence that, when the electron beam is positioned at the gap, only the antibonding modes are excited, whereas at the two ends of the dimer bonding and antibonding modes are excited.

In addition to the longitudinal modes, a mode centered at ~2.5 eV is discernible in Figure 3a. Noticeably, this mode is hardly excited when the electron beam is positioned close to the dimer gap. As for the single wire, it is efficiently excited along the wire and decays rapidly beyond the two ends of the dimer. We assign this peak to a transverse mode of the dimer. The energy is similar to that of the transverse resonance of the single wire, and the mode is much broader

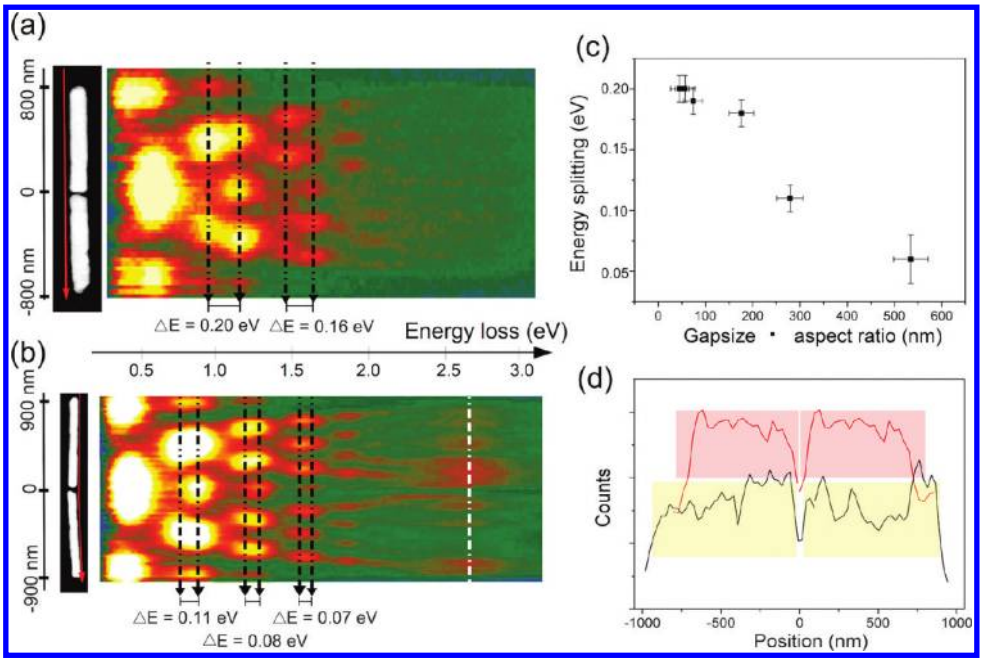

Figure 4. Plasmonic field intensity maps of two dimers with gap size ~7 nm and aspect ratio 6.5 (a) and gap size 30 nm and aspect ratio 9.3 (b). In (a) the distance between wire and scan line is on average ~30 nm; in (b) it is only ~15 nm. (c) Energy splitting *versus* gap size multiplied by the dimer aspect ratio for six different dimers. (d) Count number *versus* position along the dimers in (b) (black line) and Figure 3a (red line) at the energy of the transversal mode. The yellow and red areas represent the positions of the wires.

compared to the longitudinal ones. It is known for the nanowires that several transversal modes are very close in energy.[24] Thus, besides increased interband damping with increasing energy, an overlap of several transverse modes due to a limited energy resolution could be a possible reason for the broadening. As for the longitudinal modes, the transverse modes of a dimer split into bonding and antibonding modes,[24] leading to additional modes that could possibly further broaden the transverse peak of the dimer compared to that of the single wire.

The energy difference between two consecutive bonding modes (or two consecutive antibonding modes) decreases with increasing energy, as indicated by the red arrows in Figure 3b from 0.50 ± 0.02 eV for the difference between the $l = 1$ and the $l = 2$ bonding modes to 0.45 ± 0.02 eV for the difference between the $l = 2$ and $l = 3$ bonding modes. As mentioned above, each pair of a bonding and the corresponding antibonding mode appears to have a smaller energy difference compared to the difference to the next bonding−antibonding pair. The spectra in Figure 3a evidence that the energy difference between a pair of bonding and antibonding decreases with increasing multipole order from 0.23 ± 0.02 eV for $l = 1$ to 0.13 ± 0.02 eV for $l = 3$. This decrease with increasing multipole order confirms theoretical results of Willingham *et al.*[24] and originates most probably from the lower induced electric fields for multipole orders compared to the dipolar mode and thus weaker interaction forces between the plasmons of the two individual wires.

We observe that the energy splitting into bonding and antibonding LSP modes depends on the characteristics of the dimer. The two mappings in Figure 4a and b show exemplarily the splitting measured for two dimers with different aspect ratio and gap size. The dimer in Figure 4a consists of two wires with length 826 ± 5 and 764 ± 5 nm, respectively, a diameter of 120 ± 5 nm, and gap size of ~7 nm. The spectra are measured with an average distance from the wire of ~30 nm. In Figure 4b, the two wires have lengths of 958 ± 5 and 902 ± 5 nm, respectively, a diameter of 100 ± 5 nm, and a gap width of ~30 nm. The average distance of the scan line to the nanowire is ~15 nm. In both cases we do not consider the energy difference for the $l = 1$ bonding and antibonding modes, to avoid errors originating from the proximity of the peaks to the zero-loss peak. The very small energy differences between bonding and antibonding mode for the third and fourth order in Figure 4b are measured by extracting appropriate spectra from the mapping. The center of the antibonding peak is measured from the spectra taken close to the gap where the bonding mode is not excited. Since the bonding and antibonding modes are not excited exactly at the same spatial position along the length of the nanowire, as will be discussed in the following in more detail, the center of the bonding peak is measured at a position were the bonding mode is efficiently excited but not the antibonding mode. We observe that for the dimer in Figure 4a, having the smaller aspect ratio as well as the smaller gap size, the splitting of the higher order modes is larger than for

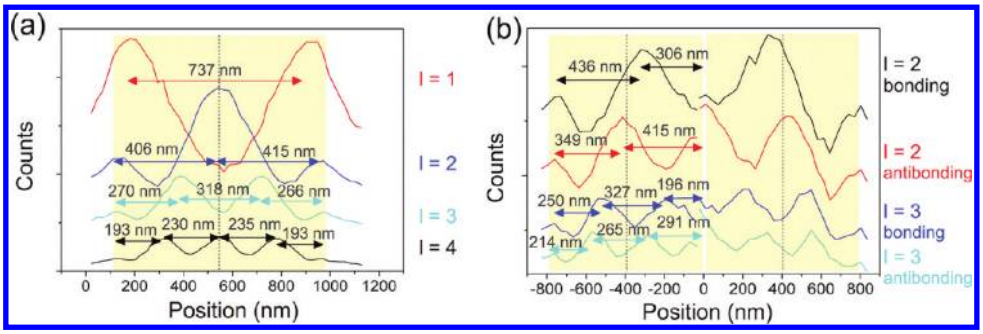

Figure 5. (a) Line scans along the nanowire for the single nanowire (Figure 1) measured at the resonance energy for the first four longitudinal LSPR. (b) Linescans of bonding and antibonding $l = 2$ and $l = 3$ modes of the nanowire dimer (Figure 3).

the dimer in Figure 4b, as expected from previous simulations that showed that the splitting increases with decreasing gap size and decreasing aspect ratio.[24,39] We plotted the energy splitting of the $l = 2$ modes as a function of gap size times aspect ratio for five different dimers in Figure 4c, confirming an increase in energy splitting with aspect ratio times gap size. Further investigations are necessary to discern the influence of aspect ratio and gap size separately. The aspect ratio of the dimer (AR) was calculated as L_d/D where L_d is the average length of both wires. In refs 40 and 41, an additional dependency on energy splitting of AR_1/AR_2 was observed, AR_1 and AR_2 being the two aspect ratios of the two wires forming a dimer. We neglect this influence since for all dimers considered in Figure 4c AR_1/AR_2 ranges in a small interval between 1.03 and 1.12.

Figure 4d shows the line scans (count numbers *versus* position) for the dimers in Figure 4b (black line) and in Figure 3a (red line) at the center energy of the transversal plasmon resonance. The line scans are also depicted in Figure 4b and Figure 3a by white dashed lines. The yellow and red areas in Figure 4d represent the positions of the wires, respectively. As already mentioned, the transversal plasmon resonance is in both cases efficiently excited along the wires but is hardly excited close to the gap. Figure 4b reveals strong intensity fluctuations of this mode. We think that these fluctuations are related to the fact that the decay length into the dielectric perpendicular to the long wire axis is very short. For the single nanowire we measured a decay length of about 20 nm, the decay length being defined as the distance at which the amplitude is reduced by a factor of e^{-1}. Thus, small diameter fluctuations of the wires together with small distance variations between wire surface and electron beam (average ~10 nm for scan line in Figure 3a and ~15 nm for scan line in Figure 4b) can account for the intensity fluctuations of this mode along the scan line. For the dimer in Figure 4a, we cannot distinguish the transversal plasmon resonance from the background since in this case the plasmonic field maps were measured at an increased distance of about 30 nm from the wire.

The three plasmon mappings in Figures 3a, 4a, and 4b show that the energy-loss maxima of bonding and antibonding modes of the same order l are not located exactly at the same spatial positions. To analyze this in more detail, we plotted in Figure 5a the line scans along the single nanowire (shown in Figure 1) at the resonance energy for the $l = 1$ (red line), $l = 2$ (blue line), $l = 3$ (light blue line), and $l = 4$ (black line) modes. In the same manner line scans are shown in Figure 5b for the nanowire dimer (Figure 3) for the following modes: $l = 2$ bonding (black line), $l = 2$ antibonding (red line), $l = 3$ bonding (blue line), and $l = 3$ antibonding (light blue line). In this case, the spectra are normalized to the zero-loss intensity. The yellow highlighted area in the figures represents the position of the wires, and the vertical dashed lines indicate the middle of each nanowire.

The count maxima in the line scans represent the positive and negative electric field maxima of the LSP modes. Thus, we can determine the surface plasmon half-wavelengths, $\lambda_{sp}/2$, of the structures by measuring the distance between two peaks. It is remarkable that in Figure 5a λ_{sp} is not constant along the whole wire, but clearly decreases when approaching the nanowire ends. This observation is in good agreement with results reported in refs 31 and 36 for silver nanowires with length 400 nm and diameter 15 nm as well as length 700 nm and diameter 50 nm, respectively. Our results evidence that similar effects occur also in gold nanowires with lengths in the μm range and larger diameters. This variation in $\lambda_{sp}/2$ along the nanowire is due to the phase shift at the wire ends (see eq 1) and decreases with increasing multipole order approaching the simplified resonator equation $L_{resonator} = (l/2)\lambda_{SP}$.

The shift in bonding and antibonding mode maxima in the case of the nanowire dimer, which was already pointed out above, is visualized in Figure 5b. A discontinuity in the profiles at the position of the gap is visible for all bonding and antibonding modes. This results from slightly different line scan-to-gap distances at the gap, caused by a very small shift between the two line scans (one along each of the nanowires forming the dimer). Measuring two line scans assured a constant distance to the wire surface along each of the

dimer wires. In contrast to the single wire, we observe in the case of the dimer that the maxima are not arranged symmetrically to the middle of the wire. For the bonding modes ($l = 2$ and $l = 3$) a shift of all maxima along the wire toward the gap is observed, whereas for the antibonding modes, the maxima shift toward the dimer ends. We attribute the shift between bonding and antibonding modes to the attraction of negative and positive charges at the opposite gap ends or to repelling of charges of equal sign for bonding and antibonding modes, respectively. In addition, we measure for the $l = 3$ bonding as well as for the $l = 3$ antibonding mode a shorter distance between the two maxima at the end of the wire than the two maxima in the middle of the nanowire. This is in analogy to the observation for the single nanowire. Whether this can be understood in the framework of phase shifts at the wire ends as for the single wire remains up to now unclear. Due to the two slightly different lengths of the wires forming a dimer, one would expect slightly different wavelengths,which cannot be quantified with the current accuracy.

CONCLUSIONS

In summary, we present high-resolution plasmonic intensity maps of a single nanowire and nanowire dimers. We investigate the excitation of longitudinal and transversal resonances depending on the electron beam positioning as well as the resonance energies depending on the nanowire aspect ratio and the gap size. The transversal resonance is not excited when positioning the electron beam by the gap and decays rapidly with increasing distance from the wire surface. The intensity maps evidence the splitting into bonding and antibonding modes of the longitudinal multipole modes of nanowire dimers up to the third order. In addition, it is revealed that the field maxima spatial positions along the nanowire dimers for each bonding and the corresponding antibonding mode do not coincide, indicating that the surface plasmon wavelength is affected not only by the geometry of the nanowire but also by the presence of nanostructures in their close proximity.

METHODS

Single nanowires and nanowire dimers were synthesized by electrochemical deposition into ion track-etched polycarbonate membranes. To fabricate the membranes, polycarbonate foils (30 μm thick, Makrofol N, Bayer) were irradiated with swift heavy ions (energy ~2 GeV) at the linear accelerator UNILAC of GSI Helmholtz Centre for Heavy Ion Research.[42−44] The diameter of the nanowires is defined by the size of the pores in the membranes and was adjusted by varying the etching time of the pores. The length of the wires was controlled by recording the current during the deposition process and stopping the process after depositing the required amount of metal. The nanowire dimers were synthesized in a two-step process. The first step was to deposit segmented gold/silver/gold nanowires by sequential potentiostatic deposition, using an electrolyte containing $Ag(CN)_2^-$ and $Au(CN)_2^-$ ions.[45] The lengths of the silver and gold segments were controlled by the duration of the corresponding pulses. The segments do not consist of pure gold or silver, but always contain a certain amount of the second metal. After dissolution of the polymer template using dichloromethane, the nanowires were dispersed in 2-propanol and subsequently dropped on a 30 nm thick silicon nitride membrane. The substrate was dried and finally dipped into concentrated nitric acid for three hours to etch out the silver segment.[46] The gap size is given by the length of the silver segment. Thus, using this method, nanogaps between 7 and 30 nm were fabricated. All gap sizes reported here have been measured at the smallest distance between two wires forming a dimer. After the nitric acid treatment of the wires, a silver content of about 30 atomic percent is measured by EDX for the gold-rich segments. We assume that the silver at the surface of the nanowires is dissolved, while only silver enclosed by gold atoms remains, playing a minor role in the determination of the surface plasmon resonance energies.[47] Therefore, the nanowires are referred to as gold wires. To remove potentially remaining small metallic connections between the gold-rich segments, some of the wires were heated to 300 °C for 30 min after dissolution of the silver.

Using the Zeiss SESAM transmission electron microscope operated at 200 kV with a field-emission gun and equipped with a MANDOLINE energy filter, LSPR were analyzed. The use of an electrostatic omega-type monochromator reduces the energy spread of the electron gun to typically 0.1 eV. In the present experiments, we used a width of 0.12 eV in order to increase the electron probe current, thus improving counting statistics. In all spectra, the zero-loss peak was subtracted by fitting a power law function to the positive energy-loss tail of this peak.

Acknowledgment. The authors would like to thank R. Vogelgesang, C. Trautmann, F. Neubrech, and A. Pucci for fruitful discussions.

REFERENCES AND NOTES

1. Moskovits, M. Surface-Enhanced Raman Spectroscopy: A Brief Retrospective. *J. Raman Spectrosc.* **2005**, *36*, 485–496.
2. Kneipp, K.; Wang, Y.; Kneipp, H.; Perelman, L. T.; Itzkan, I.; Dasari, R. R.; Feld, M. S. Single Molecule Detection Using Surface-Enhanced Raman Scattering (SERS). *Phys. Rev. Lett.* **1997**, *78*, 1667–1670.
3. Nie, S.; Emory, S. R. Probing Single Molecules and Single Nanoparticles by Surface-Enhanced Raman Scattering. *Science* **1997**, *275*, 1102–1106.
4. Neubrech, F.; Kolb, T.; Lovrincic, R.; Fahsold, G.; Pucci, A.; Aizpurua, J.; Cornelius, T. W.; Toimil-Molares, M. E.; Neumann, R.; Karim, S. Resonances of Individual Metal Nanowires in the Infrared. *Appl. Phys. Lett.* **2006**, *89*, 253104/1–253104/3.
5. Neubrech, F.; Pucci, A.; Cornelius, T. W.; Karim, S.; Garcia-Etxarri, A.; Aizpurua, J. Resonant Plasmonic and Vibrational Coupling in a Tailored Nanoantenna for Infrared Detection. *Phys. Rev. Lett.* **2008**, *101*, 157403/1–157403/4.
6. Brongersma, M. L.; Hartman, J. W.; Atwater, H. A. Electromagnetic Energy Transfer and Switching in Nanoparticle Chain Arrays below the Diffraction Limit. *Phys. Rev. B* **2000**, *62*, 16356–16359.
7. Maier, S. A.; Kik, P. G.; Atwater, H. A.; Meltzer, S.; Harel, E.; Koel, B. E.; Requicha, A. A. G. Local Detection of Electromagnetic Energy Transport below the Diffraction Limit in Metal Nanoparticle Plasmon Waveguides. *Nat. Mater.* **2003**, *2*, 229–232.
8. Talley, C. E.; Jackson, J. B.; Oubre, C.; Grady, N. K.; Hollars, C. W.; Lane, S. M.; Huser, T. R.; Nordlander, P.; Halas, N. J. Surface-Enhanced Raman Scattering from Individual Au

Nanoparticles and Nanoparticle Dimer Substrates. *Nano Lett.* **2005**, *5*, 1569–1574.
9. Li, S.; Pedano, M. L.; Chang, S. H.; Mirkin, C. A.; Schatz, G. C. Gap Structure Effects on Surface-Enhanced Raman Scattering Intensities for Gold Gapped Rods. *Nano Lett.* **2010**, *10*, 1722–1727.
10. Felidj, N.; Aubard, J.; Levi, G.; Krenn, J. R.; Hohenau, A.; Schider, G.; Leitner, A.; Aussenegg, F. R. Optimized Surface-Enhanced Raman Scattering on Gold Nanoparticle Arrays. *Appl. Phys. Lett.* **2003**, *82*, 3095–3097.
11. Felidj, N.; Aubard, J.; Levi, G.; Krenn, J. R.; Salerno, M.; Schider, G.; Lamprecht, B.; Leitner, A.; Aussenegg, F. R. Controlling the Optical Response of Regular Arrays of Gold Particles for Surface-Enhanced Raman Scattering. *Phys. Rev. B* **2002**, *65*, 075419/1–075419/9.
12. Billot, L.; Lamy de la Chapelle, M.; Grimault, A. S.; Vial, A.; Barchiesi, D.; Bijeon, J. L.; Adam, P. M.; Royer, P. Surface-Enhanced Raman Scattering on Gold Nanowire Arrays: Evidence of Strong Multipolar Surface Plasmon Resonance Enhancement. *Chem. Phys. Lett.* **2006**, *422*, 303–307.
13. Laurent, G.; Felidj, N.; Aubard, J.; Levi, G.; Krenn, J. R.; Hohenau, A.; Schider, G.; Leitner, A.; Aussenegg, F. R. Surface-Enhanced Raman Scattering Arising from Multipolar Plasmon Excitation. *J. Chem. Phys.* **2005**, *122*, 011102/1–011102/4.
14. Li, X.; Xu, W.; Zhang, J.; Jia, H.; Yang, B.; Zhao, B.; Li, B.; Ozaki, Y. Self-Assembled Metal Colloid Films: Two Approaches for Preparing New SERS Active Substrates. *Langmuir* **2004**, *20*, 1298–1304.
15. Polavarapu, L.; Xu, Q. H. Water-Soluble Conjugated Polymer-Induced Self-Assembly of Gold Nanoparticles and Its Application to SERS. *Langmuir* **2008**, *24*, 10608–10611.
16. Hao, E.; Li, S.; Bailey, R. C.; Zou, S.; Schatz, G. C.; Hupp, J. T. Optical Properties of Metal Nanoshells. *J. Phys. Chem. B* **2004**, *108*, 1224–1229.
17. Khlebtsov, B. N.; Khlebtsov, N. G. Multipole Plasmons in Metal Nanorods: Scaling Properties and Dependence on Particle Size, Shape, Orientation, and Dielectric Environment. *J. Phys. Chem. C* **2007**, *111*, 11516–11527.
18. Encina, E. R.; Coronado, E. A. Resonance Conditions for Multipole Plasmon Excitations in Noble Metal Nanorods. *J. Phys. Chem. C* **2007**, *111*, 16796–16801.
19. Bryant, G. W.; Garca de Abajo, F. J.; Aizpurua, J. Mapping the Plasmon Resonances of Metallic Nanoantennas. *Nano Lett.* **2008**, *8*, 631–636.
20. Jain, P. K.; Lee, K. S.; El-Sayed, I. H.; El-Sayed, M. A. Calculated Absorption and Scattering Properties of Gold Nanoparticles of Different Size, Shape, and Composition: Applications in Biological Imaging and Biomedicine. *J. Phys. Chem. B* **2006**, *110*, 7238–7248.
21. Lee, K. S.; El-Sayed, M. A. Gold and Silver Nanoparticles in Sensing and Imaging: Sensitivity of Plasmon Response to Size, Shape, and Metal Composition. *J. Phys. Chem. B* **2006**, *110*, 19220–19225.
22. Liu, M.; Lee, T. W.; Gray, S. K.; Guyot-Sionnest, P.; Pelton, M. Excitation of Dark Plasmons in Metal Nanoparticles by a Localized Emitter. *Phys. Rev. Lett.* **2009**, *102*, 107401/1–107401/4.
23. Prodan, E.; Radloff, C.; Halas, N. J.; Nordlander, P. A Hybridization Model for the Plasmon Response of Complex Nanostructures. *Science* **2003**, *302*, 419–422.
24. Willingham, B.; Brandl, D. W.; Nordlander, P. Plasmon Hybridization in Nanorod Dimers. *Appl. Phys. B: Laser Opt.* **2008**, *93*, 209–216.
25. Koh, A. L.; Bao, K.; Khan, I.; Smith, W. E.; Kothleitner, G.; Nordlander, P.; Maier, S. A.; McComb, D. W. Electron Energy-Loss Spectroscopy (EELS) of Surface Plasmons in Single Silver Nanoparticles and Dimers: Influence of Beam Damage and Mapping of Dark Modes. *ACS Nano* **2009**, *3*, 3015–3022.
26. Chu, M. W.; Myroshnychenko, V.; Chen, C. H.; Deng, J. P.; Mou, C. Y.; Garca de Abajo, F. J. Probing Bright and Dark Surface-Plasmon Modes in Individual and Coupled Noble Metal Nanoparticles Using an Electron Beam. *Nano Lett.* **2008**, *9*, 399–404.
27. Huang, J. S.; Kern, J.; Geisler, P.; Weinmann, P.; Kamp, M.; Forchel, A.; Biagioni, P.; Hecht, B. Mode Imaging and Selection in Strongly Coupled Nanoantennas. *Nano Lett.* **2010**, *10*, 2105–2110.
28. Aizpurua, J.; Bryant, G. W.; Richter, L. J.; Garca de Abajo, F. J.; Kelley, B. K.; Mallouk, T. Optical Properties of Coupled Metallic Nanorods for Field-Enhanced Spectroscopy. *Phys. Rev. B* **2005**, *71*, 235420/1–235420/13.
29. Dorfmüller, J.; Vogelgesang, R.; Weitz, R. T.; Rockstuhl, C.; Etrich, C.; Pertsch, T.; Lederer, F.; Kern, K. Fabry-Perot Resonances in One-Dimensional Plasmonic Nanostructures. *Nano Lett.* **2009**, *9*, 2372–2377.
30. Schaffer, B.; Hohenester, U.; Trügler, A.; Hofer, F. High-Resolution Surface Plasmon Imaging of Gold Nanoparticles by Energy-Filtered Transmission Electron Microscopy. *Phys. Rev. B* **2009**, *79*, 041401/1–041401/9.
31. Rossouw, D.; Couillard, M.; Vickery, J.; Kumacheva, E.; Botton, G. A. Multipolar Plasmonic Resonances in Silver Nanowire Antennas Imaged with a Subnanometer Electron Probe. *Nano Lett.* **2011**, *11*, 1499–1504.
32. Guiton, B.; Iberi, V.; Li, S.; Leonard, D. N.; Parish, C. M.; Kotula, P. G.; Varela, M.; Schatz, G. C.; Pennycook, S. J.; Camden, J. P. Correlated Optical Measurements and Plasmon Mapping of Silver Nanorods. *Nano Lett.* **2011**, *11*, 3482–3488.
33. Gómez-Medina, R.; Yamamoto, N.; Nakano, M.; Garca de Abajo, F. J. Mapping Plasmons in Nanoantennas via Cathodoluminescence. *New J. Phys.* **2008**, *10*, 105009/1–105009/13.
34. Bosman, M.; Keast, V. J.; Watanabe, M.; Maaroof, A. I.; Cortie, M. B. Mapping Surface Plasmons at the Nanometre Scale with an Electron Beam. *Nanotechnology* **2007**, *18*, 165505/1–165505/5.
35. N'Gom, M.; Ringnalda, J.; Mansfield, J. F.; Agarwal, A.; Kotov, N.; Zaluzec, N. J.; Norris, T. B. Single Particle Plasmon Spectroscopy of Silver Nanowires and Gold Nanorods. *Nano Lett.* **2008**, *8*, 3200–3204.
36. Nicoletti, O.; Wubs, M.; Mortensen, N. A.; Sigle, W.; van Aken, P. A.; Midgley, P. A. Surface Plasmon Modes of a Single Silver Nanorod: An Electron Energy Loss Study. *Opt. Express* **2011**, *19*, 15371/1–15371/9.
37. Garca de Abajo, F. J.; Kociak, M. Probing the Photonic Local Density of States with Electron Energy Loss Spectroscopy. *Phys. Rev. B* **2008**, *100*, 106804/1–106804/4.
38. Johnson, P. B.; Christy, R. W. Optical Constants of the Noble Metals. *Phys. Rev. B* **1972**, *6*, 4370–4379.
39. Encina, E. R.; Coronado, E. A. Plasmon Coupling in Silver Nanosphere Pairs. *J. Phys. Chem. C* **2010**, *114*, 3918–3923.
40. Slaughter, L. S.; Wu, Y.; Willingham, B. A.; Nordlander, P.; Link, S. Effects of Symmetry Breaking and Conductive Contact on the Plasmon Coupling in Gold Nanorod Dimers. *ACS Nano* **2010**, *4*, 4657–4666.
41. Huang, C.; Yin, X.; Kong, L.; Zhu, Y. Interactions of Nanorod Particles in the Strong Coupling Regime. *J. Phys. Chem. C* **2010**, *114*, 21123–21131.
42. Karim, S.; Toimil-Molares, M. E.; Maurer, F.; Miehe, G.; Ensinger, W.; Liu, J.; Cornelius, T. W.; Neumann, R. Synthesis of Gold Nanowires with Controlled Crystallographic Characteristics. *Appl. Phys. A: Mater. Sci. Process.* **2006**, *84*, 403–407.
43. Toimil Molares, M. E.; Brötz, J.; Buschmann, V.; Dobrev, D.; Neumann, R.; Scholz, R.; Schuchert, I. U.; Trautmann, C.; Vetter, J. Etched Heavy Ion Tracks in Polycarbonate as Template for Copper Nanowires. *Nucl. Instrum. Methods Phys. Res. B* **2001**, *185*, 192–197.
44. Toimil-Molares, M. E.; Buschmann, V.; Dobrev, D.; Neumann, R.; Scholz, R.; Schuchert, I. U.; Vetter, J. Single-Crystalline Copper Nanowires Produced by Electrochemical Deposition in Polymeric Ion Track Membranes. *Adv. Mater.* **2001**, *13*, 62–65.
45. Ji, C.; Oskam, G.; Ding, Y.; Erlebacher, J. D.; Wagner, A. J.; Searson, P. C. Deposition of $Au_xAg_{1-x}/Au_yAg_{1-y}$ Multilayers and Multisegment Nanowires. *J. Electrochem. Soc.* **2003**, *150*, C523–C528.

46. Hoang, N. V.; Kumar, S.; Kim, G. H. Growth of Segmented Gold Nanorods with Nanogaps by the Electrochemical Wet Etching Technique for Single-Electron Transistor Applications. *Nanotechnology* **2009**, *20*, 125607/1–125607/9.
47. Sinzig, J.; Radtke, U.; Quinten, M.; Kreibig, U. Binary Clusters: Homogeneous Alloys and Nucleus-Shell Structures. *Z. Phys. D* **1993**, *26*, 242–245.